Engineering a 3D composite hydrogel with antibacterial activity for skin regeneration

Ana Moura Vieira Faria Brites, ana.brites@tecnico.ulisboa.pt
Instituto Superior Técnico – Universidade de Lisboa | November 2021

Abstract: Wound care is a huge burden in worldwide health care expenses and the development of new therapies for topical applications is crucial. One of the developed approaches to tackle this problem is to combine composite hydrogels with three-dimensional (3D) printing technology. The main goal of this work was to produce 3D printed gelatine-based hydrogels displaying antibacterial properties, to possibly use in topical applications. To achieve this, Manuka Honey (MH), a potent antimicrobial monofloral honey, was incorporated into a gelatin-based hydrogel. The increase in gelatine concentration from 30% to 40%, as well as the incorporation of MH, were studied through rheological tests. In both cases, an increase in ink viscosity and in printing temperature, from 34ºC to 43 ºC, occurred. The remaining printing conditions, printing pressure (25 Psi), layer heigh (0.15 mm), line width (0.6 mm) and printing velocity (30 mm/s) were maintained for all inks. Reproducible three-layered patches, with high shape fidelity and adequate porosity were obtained. The MH loaded 3D printed hydrogels demonstrated significant antibacterial properties against against *S. aureus*, *S. epidermidis* and *E. coli*, but not *P. aeruginosa*, after 24h. A higher impact on gram-positive bacteria was perceived. Gelatin-base patches were not cytotoxic against human dermal fibroblasts and human epidermal keratinocytes, after 24h. Moreover, the MH concentration was a determinant factor in the cytotoxic tests. HET-CAM tests were also performed, where the patches did not induce irritation nor promote angiogenesis. These results suggest that the 3D printed hydrogels could be suitable for the development of topical applications with therapeutic properties.

Keywords: Gelatine-based hydrogel; Manuka Honey; Wound dressing; 3D printing; antibacterial activity.

1. Introduction

Injury and wound care account for around half of the world's annual health care expenses, being a significant burden to the healthcare system [1]. A key element in the treatment of wounds is the choice of the adequate therapy. An ideal wound dressing must maintain a local moist environment around the wound and stop wound desiccation; allow good gases circulation; offer a protective role against harmful bacteria and contaminants; remove wound exudates and promote tissue regeneration; possess mechanical protection and improve the overall quality of wound healing [2]. Taking the above factors into consideration, hydrogels are great candidates for wound dressings.

Hydrogels were the first biomaterials designed for use in the human body and are 3D networks formed by cross-linking hydrophilic polymer chains embedded in a water-rich environment. Its large surface network allows a physical and chemical tunability of its properties, through several mechanisms that include physical and chemical cross-linking and ionic interaction. It also allows the hydrogels to absorb up to thousands of times their equivalent weight in water until the process reaches an equilibrium state [3].

Different types of biomaterials can constitute the matrixes of the hydrogels, such as polymers derived from natural sources or synthetic sources [4]. In this work, gelatine will be used as the primary constituent of the hydrogel matrix. Gelatine, which is derived from collagen, is commonly used due to high abundance, low cost, biocompatibility, biodegradability, and low antigenicity [5]. In addition, it forms a nanofiber structure that due its large specific surface area, high porosity, and good permeability, can biomimic the extracellular matrix, favouring cell adhesion, migration, and proliferation [5].

Another important aspect of wound dressings is to additionally provide therapeutic options, such as antibacterial activity. In this study, Manuka honey (MH) was used as therapeutic agent to provide antibacterial activity to the hydrogels.

Leptospermum honey from New Zealand, known as MH has a high osmolarity and sugar content, that can provide a powerful antibacterial effect and microbial growth inhibition. Its low pH (3.5-4.5), besides contributing to microbial growth inhibition, can also stimulate macrophages and its bactericidal activity, increase fibroblast activity, increase oxygenation, and induce angiogenesis [6]. The prominent antibacterial activity of MH depends on its Unique Manuka Factor (UMF), that corresponds to the concentration of methylglyoxal (MGO) content, a potent non-peroxide antibacterial compound [6]. MH is known to be effective against a panoply of bacteria, like *Enterobacter aerogenes*, *Staphylococcus aureus* and *Staphylococcus epidermidis, Escherichia coli*, *Pseudomonas aeruginosa,* among others, and against biofilm formation [7]. This antibacterial effect is also attributed to several other components (e.g. lysozyme, bee peptides, flavonoids, phenolic acids, etc) [8]. Moreover, the low levels of hydrogen peroxide produced by MH can also affect its antibacterial activity. However, in high amounts, it can cause a deleterious effect in cells and tissues [8].

Due to these beneficial properties, some honey impregnated dressings are already available in the market, and clinical trials have shown its advantages in wound healing applications [8].

Furthermore, most current wound dressings are not customisable to suit specific conditions or provide specific therapeutic compounds. 3D printing has the potential to provide customized innovative solutions. This method allows the printing of flexible hydrogels with several layers through the conversion of computer-aided design (CAD) models into 3D complex structures [1].

The current work focuses on establishing 3D printed gelatine-based hydrogel containing an antibacterial agent, Manuka honey, crucial for wound treatment and skin regeneration. The developed patches must be reproducible, with high shape fidelity and adequate porosity. Moreover, the patches must provide an antibacterial activity, whilst being biocompatible.

2. Materials and Methods

2.1. Materials

Gelatine was obtained from Acopharma (Spain), glycerine purchased from Lacrilar (Torres Vedras, Portugal) and sucrose from Fisher Scientific (Hampton, United States). The bioactive compound, Manuka Honey (MH), was acquired from Pure Gold (New Zealand). Purified water was attained by reverse osmosis and electrodeionization (Millipore®, Elix 3), followed by filtration (filter pore 0.22 um) and sterilization. Sodium methylparaben and sodium propylparaben, known as nipagin and nipazol, respectively, were purchased from Fagron (Spain).

2.2. Preparation of hydrogel inks.

Gelatine-based inks were using the excipients described in Table 1. For easy recording, Manuka honey is abbreviated as MH and the inks with low concentration of gelatine P30 and high concentration P40.

Table 1 - Quantitative composition of Gelatine-Based Hydrogel inks.

	Identification (ID)		
Composition (%, w/w)	P30	MH-P30	P40
Gelatine	30	30	40
Glycerine	8	8	10
Sucrose	2	-	10
Water	59.8	19.8	39.8
MH	-	40	-
Nipagin	0.18	0.18	0.18
Nipazol	0.02	0.02	0.02

First, a certain amount of glycerine (Table 1) is weighted with distilled water and the mixture is heated at 40 ºC for 5 minutes in the water bath. For the gelatine-based hydrogel with MH (MH-P30), the incorporation of the MH is also made during this step. Afterwards, gelatine, sucrose, nipagin and nipazol are weighted (Table 2.1) and added to the previous mixture. Then, the hydrogel is kept in a water bath at 40°C for 45 min, to guarantee the homogenization of the ink.

2.3. Rheological Characterization of Inks

Gelation temperature of the inks was determined by a single frequency strain-controlled temperature event sequence. Measurements were carried out with a plate–plate geometry and a gap of 0.5 mm (patch height simulation) in a stress Kinexus Lab+ Rheometer (Malvern Instruments, Malvern, UK). The onset of gelation temperature was defined as the crossover, where the data point showed the gel-sol transition (G'>G"). Measurements were performed from 50 °C to 25 °C at a rate of 2.5ºC/min; frequency was kept at 1 Hz and the shear strain at 1%.

2.4. Production and Characterization of 3D printed Gelatine-Manuka Hydrogel patch

The 3D printed gelatine-based patches were printed with an Allevi 2 printer. The inks were extruded through specific nozzles, with 27 Gauge and an inner diameter of 0.200 mm for P30 ink and 25 Gauge and inner diameter of 0.250 mm for MH-P30 and P40 inks. Three-layered patches were developed, each layer with 45º angle difference. The optimized printing parameters for each gelatine-based hydrogel ink are described in Table 2.

Table 2 - Printing parameters used for each ink.

Identification (ID)	P30	MH-P30	P40
$T_{chamber}$ (ºC)	26	26	26
$T_{cartridge}$ (ºC)	34	43	43
Pressure (Psi)	25	25	25
Line Width (mm)	0.6	0.6	0.6
Layer Height (mm)	0.15	0.15	0.15
Printing Velocity (mm/s)	30	30	30

After optimization of the gelatine-based hydrogels ink and the printing conditions, it was selected the characteristics and composition of each hydrogel to be studied (Table 3).

Table 3 - Characterization and a detailed description of all 3D printed hydrogels ought to be studied.

Identification (ID)	**Layers Description**
P30	3 layers of P30 ink
3MH-P30	3 layers of MH-P30 ink
2MH-P30	Layer 1&3 of MH-P30 ink and layer 2 of P30 ink
P40	3 layers of P40 ink

2.5. 3D patches physico-chemical characterization

The morphology of the 3D hydrogel patches, and porosity were examined using a scanning electron microscope (SEM Hitachi, Tokyo, Japan). To increase conductivity, the 3D patches were coated with a thin layer of gold/palladium and examined using an acceleration voltage of 20 kV. Pore size diameter was analysed using ImageJ® software and pore size was determined as mean pore size (µm) ± S.D. To identify the functional groups of the 3D patches, attenuated total reflectance-Fourier transform infrared spectroscopy (ATR-FTIR) spectra were acquired using a Nicolet FTIR spectrometer (Thermo Electron, Thermo Fisher Scientific, Waltham, MA, USA). The 3D patches and respective raw materials were placed on the ATR diamond crystal, and spectra were obtained in the range of 500 to 4500 cm^{-1} with a resolution of 8 cm^{-1}. The recorded signals were reported as transmittance.

2.6. Biological Characterization of Bioactive 3D patches

For the biological characterization, the focus was on the hydrogels' composition, to confirm its possible antibacterial activity and regeneration capacities. Prior to its use, the 3D printed hydrogels were sterilized under UV light for 30 minutes, on each side.

2.6.1. *In vitro* antibacterial evaluation of bioactive 3D patches

Dose-Response Curve of Manuka Honey

The minimum inhibitory concentration (MIC) and minimum bactericidal concentration (MBC) of 4 bacterial strains were assessed for the incorporated MH. Gram-negative bacteria *Escherichia coli* ATCC 25922 and *Pseudomonas aeruginosa* PA01; gram-positive bacteria *Staphylococcus epidermidis* RP62A and *Staphylococcus aureus* ATCC 25923 were the chosen strains, due to their importance in the wound healing. For MIC determination, MH was serially diluted 1:2 in Tryptic Soy Broth (TSB, Liofilchem) growth medium in microdilution trays, with concentrations ranging from 0.024 to 0.5 mL MH/mL and in a total volume

of 100 µL. Each well was inoculated with 50 µL of bacteria, to yield a final bacterial concentration of $5x10^5$ CFU/mL [9]. Afterwards, the plaques were incubated at 37 °C for approx. 24 h. The MIC was defined as the lowest concentration that completely inhibited the growth of the bacterial isolates as detected by the unaided eye (first well where no turbidity was seen). MBCs were determined by subculturing, onto agar plates 10 µL of aliquots from wells containing antimicrobial concentrations greater than or equal to the MIC. Plates were incubated at 37 °C for 24 h, and viable colonies were counted. The MBC was defined as the lowest concentration at which there was no visible bacterial growth. The entire test was performed in triplicate and the results are presented admitting a MH density of ρ_{MH} = 1.42 g/mL [10].

Antibacterial activity of the 3D printed hydrogel patches

Wells without the 3D printed hydrogels were selected as the positive control and tryptic soy broth (TSB, Liofilchem) was used as a nutrient source. Three methods of antibacterial activity assessment were performed: spectrophotometer method of optical density (OD) measurement, culture-based counting for colony-forming units (CFU) and *in vitro* metabolization of resazurin.

In each well, 0.5 mL of a $1x10^5$ CFU/mL bacterial suspension was added, in 24-well plate. Next, the patches were added to each respective well and incubated for 3h, 6h and 24h at 37 °C, with continuous shaking (100 rpm). At each time point, 50 µL of each bacterial suspension was collected and transferred to a 96-well plate, to measure cell density, DO, and resazurin reduction. At each time point, the DO was measured at 600 nm using a microplate reader (BioTek® Synergy HT) to monitor bacterial growth. After OD reading, to each well, 10 µL of resazurin solution (Sigma) are added and the plaques were incubated at 37 °C, until a shift in colour was perceived. The fluorescence is read at a microplate fluorometer (BioTek® Synergy HT) equipped with a 530 nm excitation / 590 nm emission filter set. At each time point, 20 µL of the bacterial suspensions are also retrieved and placed in a 96-well plate, where sequential dilutions were performed (between 10^0 -10^{-8}) for CFU count. 10 µL of the undiluted and diluted suspensions were plated on agar Petri dishes and incubated at 37°C for 24h. 70 µL of TSB medium were introduced to replace the removed medium, at each time point. All samples were performed in triplicates.

Data from OD measurement is represented as bacterial growth (%), Equation 1; from resazurin metabolization as relative units of fluorescence (RUF) and fluorescence average, calculated by Equation 2; and for CFU count as CFU's/mL.

$$Bacterial\ Growth\ (\%) = \frac{OD\ (600\ nm)_{sample}}{OD\ (600\ nm)_{control}} x\ 100 \qquad 1$$

Where OD_{sample} and $OD_{control}$ correspond to the optical density at 600 nm of the respective sample and the control, respectively.

$$RFU\ = \frac{Fluorescence\ of\ exposed\ cells}{Fluorescence\ of\ non-exposed\ cells} \qquad 2$$

Where the fluorescence of exposed bacterial cells and non-exposed cells corresponds to the fluorescence read at 530 nm excitation / 590 nm emission of each well incubated with the 3D patches and wells with normal growth conditions, respectively.

Agar disk-diffusion method

A version of the agar disk-diffusion method was performed. Briefly, tryptic soy agar media plates, prepared from TSB (Liofilchem) and powder agar (Liofilchem), were inoculated with a concentration of $1x10^8$ CFU/mL) and spread uniformly. The tests were done against the previously used strains. Then, 3D patches were cut into 10 mm radius circles. The same was done to the agar plates, to add the 3D patches inside. The plates were incubated under suitable conditions. After 24 hours, the diameters of inhibition growth zones are measured. The level of complete and partial growth around the sample was evaluated. The test was performed in triplicate and the values correspond to average ± S.D.

2.6.2.Cell Culture

Human dermal fibroblasts (HDF) and human epidermal keratinocytes (HEK) were cultured in alpha-minimum essential medium (***α***-MEM) (Gibco,Thermo Fisher Scientific,Inc.), and Ham's Nutrient Mixture F12 (Sigma) , respectively. Both media were supplemented with 10% heat-inactivated fetal bovine serum (FBS-HI, Gibco, Brasil) and 1% Antibiotic-Antimycotic (Anti-Anti, 100X; Gibco®). Cells cultivated in T-flasks, and well-plates were incubated at 37°C, 5% CO_2 and in a humidified atmosphere.

Cell proliferation/cytotoxicity assay

The cytotoxicity of the 3D patches was evaluated on the stated cell lines. In 24-well plates, the cells were seeded in 0.5 mL/well at a concentration of $1x10^5$ cells/mL and incubated for 24h. Since the samples easily dissolve at 37 ºC, the preparation of leachates was previously done and then incubated into the cells. Each patch was placed in 0.5 mL of the respective complete medium. After the 24h incubation and adherence to the wells, the culture medium was replaced with the leachates. The cells were then incubated for 6h and 24h with the extracts.

MTT assay: Used to evaluate cytotoxicity after the incubation periods. 10% of the MTT reagent was added to each well and the plaques were incubated for 2h. To quantify cell viability, 200 µL of dimethyl sulfoxide solution (Sigma) was added for 15 minutes. Absorbance at 550 nm was measured on a microplate reader (BioTek® Synergy HT). The entire test was performed in triplicates and the obtained values correspond to Viability (%) ± S.D (%), (Equation 3).

$$Viability\ (\%)\ = \frac{OD\ (550\ nm)_{sample}}{OD\ (550\ nm)_{control}} x100 \qquad 3$$

Immunofluorescence staining protocol: In different 24-well plates, after 24h, a specific cell marker for each cell line, the cell nuclei, and the F-actin filaments were stained.

First, the wells are aspirated and washed with PBS. After PBS removal, enough formaldehyde (Sigma) to cover the well was added and incubated in the cells for 15 minutes. After formaldehyde removal, the wells are washed with PBS (Sigma). Then, PBS containing 0.1% (v/v) Triton X-100 (Sigma) was added and incubated for 20 minutes, at room temperature. After Triton removal, cells were incubated with 1% BSA (Sigma) in PBS for 30 min. After BSA removal, the rest of the protocol was performed in a dark room. The cells were incubated in the diluted primary antibody in 1% BSA in PBS overnight, at room temperature. For HDF, a mouse monoclonal Ki-67 primary antibody (1:100, Santa Cruz Biotechnology, Inc). For HEK a mouse monoclonal cytokeratin 5 primary antibody, CK5

(1:100, Santa Cruz Biotechnology). The next day, the primary cell markers were removed, and the wells were washed 2 times with PBS. Afterwards, cells were incubated with the Alexa Fluor 594 secondary antibody, a goat anti-mouse igG antibody (500 µg/mL, BioLegend), in 1% BSA for 2 h at room temperature. After 1 more wash with PBS, the F-actin filaments were stained for 30 minutes with Alexa Fluor 488 (1:100, add ref) in 1% BSA. Finally, after F-actin marker removal and 1 PBS wash, the nuclei were also stained for 15 minutes, at room temperature, with Hoechst 33342 antibody (8 µg/mL, Sigma) in PBS. The marker was removed, and the wells washed with PBS. Images of the stained cells were acquired using the Selena S digital imaging system (Logos Biosystems).

Scratch wound healing migration assay

Cells were seeded onto 24-well plates and cultured until 90-100% confluence. Without removing the medium, the created monolayer was wounded by scraping it with a 10 µL sterile pipette tip. The, each well was washed 2 times with sterile PBS and one time with non-supplemented culture medium. As before, the samples were previously diluted until dissolved in 0.5 mL of complete medium and the leachates were added to each well. Wells with only complete medium were selected as the positive control group, to compare the rate of wound healing process.

The migration was monitored by a microscope after approx. 16h and 24h. The area of the wounds was compared with the wound area at time 0, to evaluate the migration rate of cells. The distance was determined by measuring the cleared space between the wound edges with image analysis of the pictures obtained with a digital camera from an inverted microscope at 40x objective and the NIH ImageJ software. The percentage of wound closure was calculated using Equation 4,

$$Wound\ Closure\ (\%) = \left(1 - \frac{D_T}{D_0}\right) x\ 100 \qquad 4$$

Where D_T is the distance between two vertical lines at said time point after adding the extracts and D_0 is the distance between two vertical lines at time 0h in the absence of wound healing compounds.

Triplicate samples were used for this analysis and five random distances of each were used for the quantitative analysis. The results appear as Wound Closure (%) ± S.D.

Antioxidant Activity Assay

The intracellular production of reactive oxygen species (ROS) inside the cells was evaluated using a fluorometric technique by using 5(6)-carboxy-2',7'-dichloroflourescein diacetate (5(6)-CDCFDA), a fluorogenic reagent that detects reactive oxygen species. The cells were seeded onto 96-well plates at a concentration of $1x10^5$ cells/mL in 100 µL in each well and incubated for 24h to allow adherence to the wells. After the 24h, the cells were incubated for 30 minutes with 10 µM of 5(6)-CDCFDA (Enzo), in the dark at 37°C. As before, the samples were previously diluted until dissolved in 0.5 mL of complete medium and the leachates were added to each well. The leachates were placed directly in the wells (100 µL) and ascorbic acid (AA) was used as positive control (1mg/mL) and the plaques were incubated. Oxidative stress was induced by hydrogen peroxide (H_2O_2) (500 M) for 15 minutes and the ROS levels were determined at an excitation wavelength of 485 nm and emission wavelength of 520 nm, using a microplate fluorescence reader. Seven replicates were used for each hydrogel and data is shown as relative units of fluorescence (RUF) and fluorescence average. Relative units of fluorescence are calculated according to Equation 2.

***In vivo* irritation potential and angiogenic test by the HET-CAM Assay**

The 3D patches were tested for the irritation and angiogenic potential using the chorioallantoic membrane (CAM) assay according to the Interagency Coordinating Committee on the Validation of Alternative Methods (ICCVAM) guidelines add guideline. Freshly laid fertilized chicken eggs were incubated horizontally at 37 °C in a 60% humidified atmosphere, using an Octagon Advance incubator (Brinsea) with one hour scheduled rotation. At day 8-post fertilization, a small window was made in the eggshell, under aseptic conditions, to gain access to the CAM beneath. The samples were placed randomly and individually on the CAM of the chicken embryo. For a contact period of 0.5, 2.0 and 5.0 min, the CAM was assessed by visual inspection and photographed with a stereomicroscope (ZEISS Stemi 305) attached to a digital camera (Axiocam 208 color, ZEISS), for signs of irritation. The irritation potential was evaluated by the occurrence of specific reactions to the membranes and/or vessels (i.e. hyperaemia, haemorrhage, clotting and changes in small vessel diameter) which were then interpreted in comparison to a negative (0.9% NaCl) and a positive (0.5M NaOH) control according to the guideline.

For the angiogenic response, after 8 days, filter paper discs (0.5 cm diameter) impregnated with the extracts were placed on the CAM. The eggs were further incubated for 3 days. The CAM surrounding the discs was cut off and photographed with a stereomicroscope (ZEISS Stemi 305) attached to a digital camera (Axiocam 208 color, ZEISS). Images were processed with the ImageJ software. Sterile saline was used as the control.

Statistical Analysis

Statistical analysis of the results referent to the biological characterization of bioactive 3D patches was performed using Microsoft Excel 365. Comparison of the experimental conditions was performed by the t-test and the comparison of several groups performed by the one-way analysis of variance (ANOVA). P-values ≤0.05 were considered significant.

3. Results and Discussion

Rheological properties of gelatine-based hydrogels inks

After the inks' development and preparation, the rheological properties of the inks were studied, to aid the printing process of the hydrogels (results not shown). The sol-gel transition temperature, Tsol-gel, from solution to an elastic network formation was determined, which indicates at which temperature the hydrogels should be printed.

Briefly, the increase in concentration of the base formulation excipients, particularly gelatine, increased the Tsol-gel from 35 ºC in P30 to almost 42 ºC in P40 ink. Ink viscosity also increased. This has been previously described by other authors [11,12]. These results suggest that the temperature inside the cartridge during printing should be higher in the P40 ink, as compared to P30. Considering that the ΔT between the temperature inside the cartridge and room temperature is 16ºC and 9ºC for P40 and P30, respectively, it is expected that the filaments spreading in P40 will be lower than P30, leading to a higher printing accuracy and more uniform and

reproductible 3D patches [13]. It is also expected the need to use a higher temperature for P40 than the indicated, since the high ΔT can cause premature gelling inside the nozzle at sol-gel transition temperature.
The results for MH incorporation on gelatine-based hydrogel ink revealed that, it was only possible to blend a maximum of 40% MH in the P30 ink, without compromising the hydrogels properties. Regarding P40 ink, due to the higher viscosity, it was not possible to add MH in percentages superiors to 20% since with higher concentrations, gelatine was not able to be dissolved and a lumpy heterogeneous paste was formed, thus this option was discarded. The addition of MH to the P30 ink did not change the gel-sol transition (~35ºC), when compared to the P30 ink. However, higher viscosity of the ink at gelation temperature was perceived. The higher ink viscosity suggests that for printing, a higher temperature than the sol-gel must be provided, since with higher viscosities in unstable temperatures, like the sol-gel transition, nozzle clogging, irregular flow rates and inhomogeneity can occur [14].

Development of 3D Gelatine-Manuka Honey Hydrogel Patches

Temperature is one of the most critical factors affecting the printability of 3D patches, since it changes the material´s intrinsic properties [15]. Filament drop tests showed optimal printing temperatures of 34 ºC for P30 and 43 ºC for MH-P30 and P40, forming a continuous and homogeneous strand. For P40, a higher printing temperature translates into an increase in filament homogeneity and quality. These results were in line with the rheological observations, i.e., for high viscous solutions, lower or equal temperatures than sol-gel can induce a gelation inside the nozzle which causes difficulties in the printing process and the formation of inhomogeneous filaments. For MH-P30, due to its viscosity, this difference is even bigger, when compared to the Tsol-gel obtained with the rheological tests. For the less viscous ink, P30, since the ΔT between the temperature inside the cartridge and the room temperature is much lower, the hydrogel is possible to be printed closer to the sol-gel transition temperature since gelation is not as sudden. Bu using the previously described printing conditions, 3-layered patches were attained. (Figure 1).

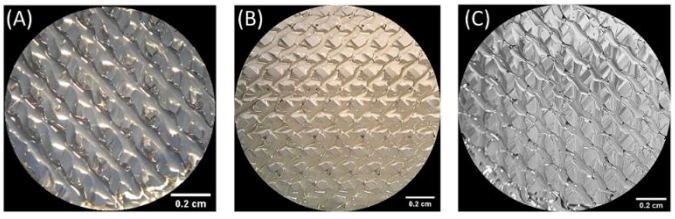

Figure 1 - Microscopic image of the developed 3D hydrogels. P30 (A); MH-P30 (B); P40 (C) printed hydrogels. Each hydrogel is composed by 3 layers of each ink.

As demonstrated by optical images the thickness of the printed strands in the 3rd layer are higher in the P30 patches when compared with MH-P30 and P40 which translates in lower printing accuracy. In addition, it was found that the quality of the 3D patch increased after the addition of MH (Figure 1B) in MH-P30 and gelatine (Figure 1C) in P40. Thus, the pores have better definition in MH-P30 and P40 with lower filament spreading when compared with P30. These results are consistent with other studies, where the addition and increased concentration of gelatine reduced the width of printed strands, increased printing accuracy and, consequently, spreading of the ink no longer occurred [5].
To further extend the MH-P30 and P40 patches characterization, the topography by SEM images of the MH-P30 and P40 patches was obtained (Figure 2).

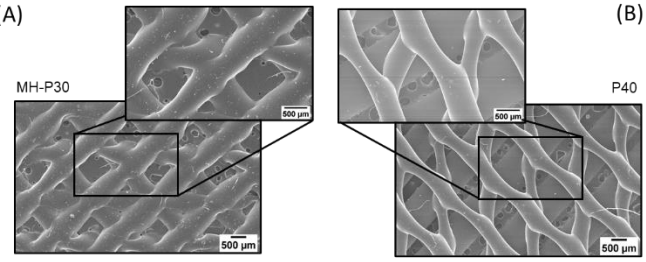

(C)

3D printed hydrogel	Mean Pore Size ± SD (µm)
MH-P30	459 ± 225
P40	517 ± 275

Figure 2 - Scanning electron microscopy (SEM) images of MH-P30 and P40 3D patches. SEM images of MH-P30 patch (A); SEM images of P40 patch (B); Mean pore size distribution (C) of the developed 3D patches.

It is instantly noticeable the low filament spreading of the bottom layer of the MH-P30 (Figure 2A), compared to the P40 (Figure 2B). The MH-P30 shows an expected line width (approx. 0.6 mm), while P40 patch presents a line width of almost double of the expected (approx. 1.1 mm). This behaviour switches in the deposition of the 2nd and 3rd layers. It is important to point out that different materials have different surface adhesion. Bed adhesion is directly linked to the wettability properties of the hydrogel ink and it has been previously stated that can drastically influence the quality of the final patch [16]. Thus, here, the introduction of MH can be increasing surface adhesion to the plastic plate, whilst in the gelatine-only patch, P40, this adhesion is lower, provoking a superior filament spreading in the first layer and less printing accuracy.
Overall, the MH-P30 hydrogel strands appear to be more uniform between layers and a more homogeneous porous structure is obtained (Figure 1A), with a mean pore size of 459± 225 µm. Considering the obtained porosity for P40, bigger, with an irregular shape and more heterogenic size pores were obtained, with an average pore diameter of 517± 275 µm. The size of the attained porous here are between a previously described range, thus, suggesting that the produced 3D patches can provide a good base for fibroblast affinity and proliferation [17]. Moreover, highly porous biomaterials are very desirable for the easy diffusion of nutrients and waste products.
From the obtained results, it can be confirmed that it is possible to develop 3-layered 3D patches, through the previously optimized conditions, to create accurate and reproducible multi-layered porous 3D patches.
Finally, ATR-FTIR analysis confirmed the presence of gelatin and MH in the patches, with all the expected peaks (results not shown).

Antibacterial activity of bioactive 3D Patches

First, the used 40% MH concentration was tested to see if it is enough to provide bacteriostatic and bactericidal activity against the studied strains. To evaluate this assumption, the minimum inhibitory concentration (MIC) and minimum bactericidal concentration (MBC) of MH on each bacterial strain was assessed. Table 4 shows the obtained results.
The results confirm that the bioactive MH has bacteriostatic and bactericidal effect for all the bacterial strains tested. A lower MIC was observed for *S. aureus*

(17.8% w/v) and equivalent MICs were found for *S. epidermidis*, *E. coli* and *P. aeruginosa* (35.5% w/v). More diluted solutions did not present activity against the different bacteria.

Table 4 - Minimum inhibitory concentration and minimum bactericidal concentration of MH for each bacterial strain tested: *S. epidermidis*, *S. aureus*, *E. coli* and *P. aeruginosa*.

Bacteria	MIC (%, w/v)	MBC (%, w/v)
S. epidermidis	35.5	35.5
S. aureus	17.8	35.5
E. coli	35.5	35.5
P. aeruginosa	35.5	35.5

Regarding the MBC concentrations, only at percentages higher than 35.5% w/v, MH was able to provoke a bactericidal effect on the viable bacteria population. No significant differences between gram-negative and gram-positive bacteria susceptibility to pure MH were encountered. Thus, it is expected that the use of 40% w/v MH in the hydrogels will have both bacteriostatic and bactericidal effect in the studied bacteria, since this value is higher than the MICs and MBCs obtained.

After confirming that the used MH percentage can provoke bacterial inhibition, the antibacterial activity of the printed hydrogels was assessed (Figure 3). The use of patches with 2 different MH concentrations was also studied. Patches with 40% w/v and ~27% w/v of MH were used, corresponding to 3MH-P30 and 2MH-P30. This decision was made to have a condition with a percentage close to the attained in the previous test and a percentage closer to the obtained in the literature.

Overall, the honey incorporated patches have a negative effect on microbial growth and viability on both gram-positive bacteria and on *E. coli*. Surprisingly, no differences were observed, comparing the different honey concentrations incorporated, the outcomes being very similar for both conditions. A higher antibacterial effect for the bacterial suspensions incubated with 3MH-P30 than with 2MH-P30 was expected, due to honey decreasing from 40% to ~27%, however, this was not seen.

Furthermore, P40 also appears to impact the gram-positive bacteria's normal growth. This can be due to a slower adaptation of the cells to the medium, caused by a higher saturation due to the added excipients, instead of an antibacterial effect. However, none of the 3D patches seem to present an inhibitory effect on *P. aeruginosa*. It is possible that the used MH concentrations in the hydrogels are too low, since the highest concentration used 40% w/v is very close to the MIC obtained (35.5% w/v).

It has been previously reported that MH has a higher antibacterial activity against gram-positive bacteria than gram-negative bacteria, which correlates to the present results [18].

Lastly, the agar diffusion method assay was performed to see if the samples could provoke bacteria inhibition and death, in a different environment and the results are described in Table 5. The results show that only the patches containing honey showed bacterial inhibition in the agar plate. The behaviour correlates to the antibacterial assay, where the gram-positive bacteria seem to be more susceptible to MH than gram-negative, as observed in 3MH-P30 hydrogels caused a wide full clearance in gram-positive bacteria and partial clearance in *E. coli*. After 24h of incubation, *S. epidermidis* showed the highest susceptibility to honey and for *E. coli* only partial clearance was reached.

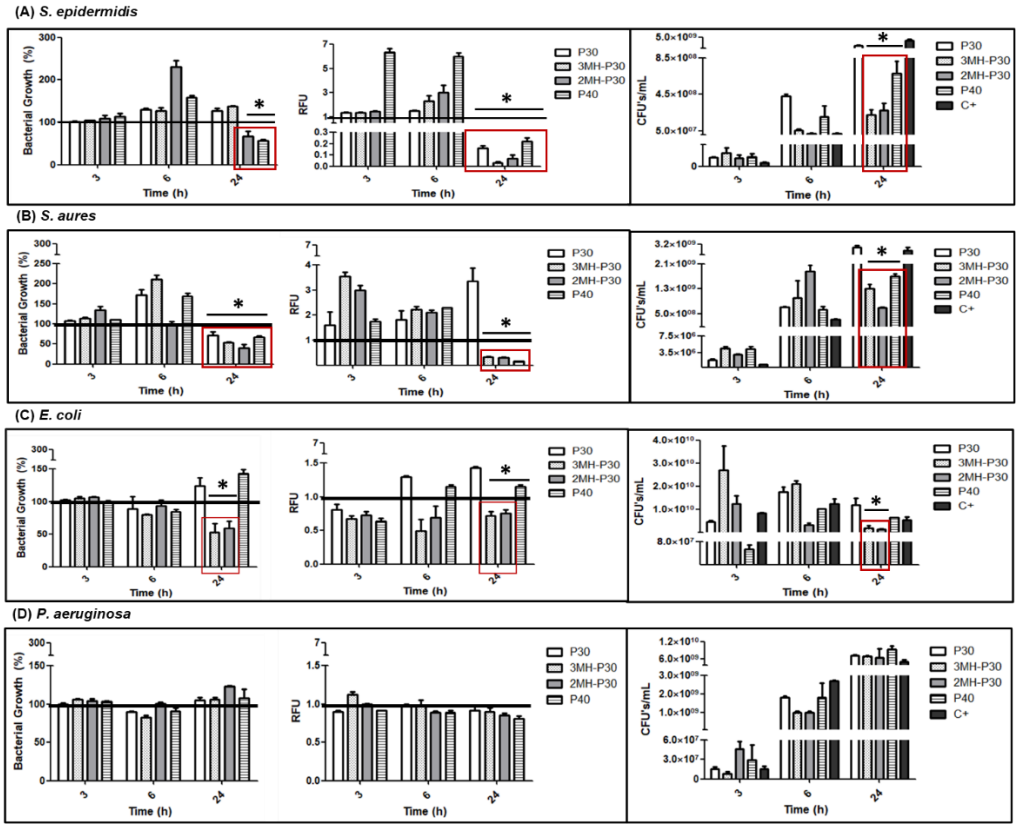

Figure 3 - Antibacterial activity of 3D hydrogels against four bacteria strains, after 3h, 6h and 24h of incubation. Bacterial growth in normal culture conditions, positive control, is indicated as 100% of bacterial growth (solid line); Resazurin reduction in normal culture conditions, positive control, is indicated as RFU = 1 (solid line); CFU counting is used to estimate the number of viable bacteria in a sample. Antibacterial activity of *S. epidermidis* (A), *S. aureus* (B), *E. coli* (C) and *P. aeruginosa* (D). * - Results lower and significantly different from the control (C^+) in normal growth medium, at 24h.

Table 5 - Agar diffusion test. The patches were placed on plates of *S. epidermidis*, *S. aureus*, *E. coli* and *P. aeruginosa* for 24 h to measure partial (*) and full clearance. Gentamicin was used as control. Note: diffusion attributed to the water content of the 3D patches was not marked.

	Studied Samples (mm)				
Bacterial Strain	P30	3MH-P30	2MH-P30	P40	Gen
S. epidermidis	Ø	20	Ø	Ø	30
S. aureus	Ø	17	Ø	Ø	30
E. coli	Ø	29±2*	29±2*	Ø	27
P. aeruginosa	Ø	Ø	Ø	Ø	35

2MH-P30 hydrogel only provoked partial clearance to *E. coli* and no inhibition was seen for the gram-positive bacteria, contrary to what was expected from the previous antibacterial activity results (Figure 3.9). As previously demonstrated, no effect was seen in *P. aeruginosa*.
When compared to gentamicin inhibition, it is interesting to note that 3MH-P30 hydrogel can provide around 67% and 57% complete inhibition to *S. epidermidis* and *S. aureus*, respectively.
These obtained results also reinforce that it is possible to successfully incorporate MH, whilst maintaining its desired properties and that the concentration of MH incorporated can affect the patches' antibacterial effect.

Biocompatibility Tests

The 3D patches have the main goal of being antibacterial agents, however, it is also important that they do not affect the viability of the cells. Therefore, a cytotoxicity assay was performed, to see the impact of the patches' composition in the human dermal fibroblasts (HDF) and human epidermal keratinocytes (HEK), shown in Figure 4.

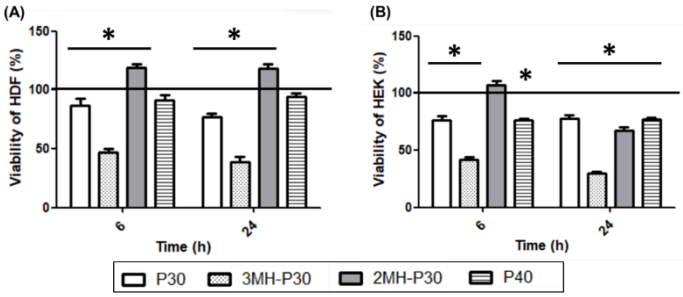

Figure 4 - MTT cytotoxicity assay. Solid line corresponds to the growth of the positive control, C^+, incubated under normal conditions. Results for human dermal fibroblasts (A) and human epidermal keratinocytes (B). * - Results significantly different from the control (C^+) at the same time point.

For HDF, the results show that 3MH-P30 extract appears to cause a reduction in viability of approx. >50% in HDF, in both time points. The composition of the 2MH-P30 patch revealed to be the most favourable of all. It even seems to be able to induce cell growth and proliferation of about more 20%, compared to the positive control. The viability reduction observed with the 3-layered patch is no longer seen. This means that a reduction in honey concentration, leads to a suitable environment for proliferation, or regeneration, in the wound context, and the viability of the cells is not compromised. The remaining extracts, P30 and P40, presented a viability of >77% and >91%, respectively, throughout the whole essay.
In HEK, similar results to HDF can be perceived. A reduction of more than 50% in cell viability is also detected, like in HDF. At 6h, the 2MH-P30 extract seems to have the same effect as in the HDF (increase in ~8% viability compared to the control), it seems to create a suitable environment for cell proliferation, possibly meaning regeneration in a wound setting. However, at 24h after incubation this is no longer observed, attaining a viability of ~70%. For P30 and P40 hydrogels' extracts, a viability higher than 76% was attained throughout the essay time.
According to the norm ISO 10993-5:2009, that describes methods to assess the in vitro cytotoxicity of medical devices, if viability is reduced to <70% of the positive control, it has a cytotoxic potential [19]. All the hydrogels appear to not provoke a cytotoxic effect in both cell lines, except for the 3MH-P30. The composition of the patch caused the viability of the cells to be reduced to less than 50%. The remaining patches composition can be categorised as non-cytotoxic. Previous studies have shown that concentrations of MH, as low as 5%, can be cytotoxic in vitro. This is hypothesized to be due to the acidic pH of MH and the closed-off environment, leading to an osmolarity deregulation of the medium [20]. In 3MH-P30 environment this could be happening.
These results were also confirmed via immunofluorescence staining. Figure 5 shows the results of the immunofluorescence assay for HDF and for HEK, at 24h after incubation.
Cultures of HDF, are accordant with the previous cytotoxic assay, where 3MH-P30 patch appears to be cytotoxic to the cells (Figure 5B) and the other samples allow a normal growth (Figure A, C-E). No Ki67 or actin staining are observed, and cellular nuclei staining is very sparse when the cells are incubated with the 3MH-P30 patch (Figure 5B). The F-actin cytoskeleton is a critical cell structure crucial not only in cellular functions (division, gene expression, intracellular transport and signalling pathways) but also in motility and differentiation mechanisms. Due to its importance, F-actin cytoskeleton is considered an early indicator of cytotoxicity [21]. Thus, it was expected to see deleterious effects on this structure, as was confirmed (Figure 5B). Considering cell morphology, HDF in the remaining conditions demonstrated flat, spindle-like, and spreading morphology (Figure 5A, C-E). High cellular density with elongated actin filaments between cells and cell-to-cell contact is also seen, as well as prominent nuclei were also evident (Figure 5A, C-E).
A reliable and specific marker for HDF has yet to be found. Other markers for other cell lineages have been used to identify HDFs [22]. Ki67 is a nuclear protein and well-established marker of cell proliferation during wound repair. It is present in actively proliferating cells and lacking in resting cells [23]. The intranuclear staining of Ki67 marker in red can be seen in wells incubated with P30, 2MH-P30 and P40, but not in the 3MH-P40 nor the control. This means that the incubation with the patches allows the cells to actively proliferate. A higher Ki67 staining is also noticeable in cells incubated with 2MH-P30 extract, which correlates to the previous results, where a higher proliferation, when compared to the control was observed (4A). Thus, for HDF, the 2MH-P30 condition appears to be the most favourable of all.
Looking at the results for HEK (Figure 5i-v), for every condition except 3MH-P30, the cells form colonies exhibiting the distinctive cobblestone morphology anticipated from primary keratinocytes *in vitro* [24].
Images of triple staining (cytoskeleton, CK5 and nuclei) are consistent with a healthy appearance of the exposed keratinocytes.

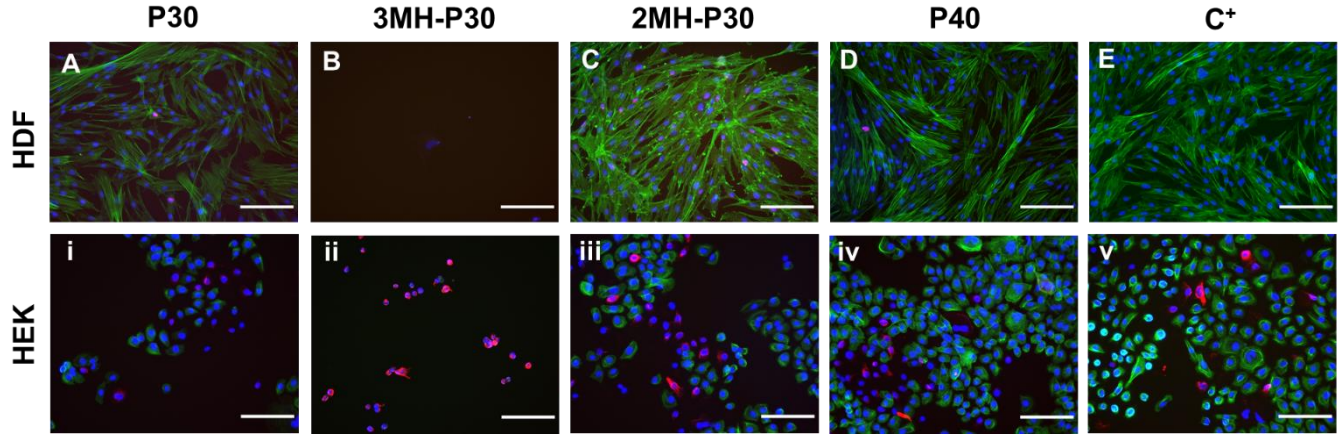

Figure 5 - F-actin (green) and nuclei (blue) staining of HDF (A-E) and HEK (i-v). Staining of the specific cell marker ki67 and CK5 (red) was also performed for HDF (A-E) and HEK (i-v), respectively. Pictures were acquired by fluorescence microscopy and scale bar represents 5 µm.

HEK are significantly smaller cells, when compared to HDF. As expected, 3MH-P30 shows a significant reduction in cell viability and the cells are dispersed, not forming the typical colonies. It is also interesting to note that the CK5 cytokeratin is expressed in the stained cells, however, the F-actin filaments were not fully developed nor were able to be observed. For the cells incubated with the remaining patches, a proper nuclei, F-actin, and specific cell marker can be seen. Additionally, the cells have staining of the specific cell marker, CK5, meaning their able to proliferate, under the imposed conditions.

Since MH also is known for its regenerative capacities and since it has been previously proved that it can increase fibroblast and keratinocytes migration, a wound scratch assay was performed (Figure 6).

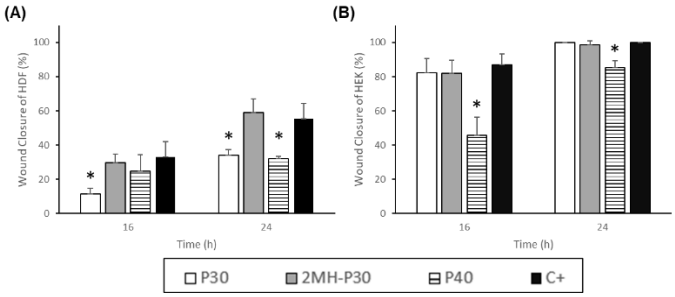

Figure 6 - Wound scratch assay *in vitro.* Wound closure was measured at 16h and 24h for human dermal fibroblasts (A) and human epidermal keratinocytes (B). * - Significantly different results from the positive control (C^+), at the same time-point.

It appears that HDF cells have a much slower migration, compared to HEK cells. None of the conditions for HDF was able to fully close the wound, during the assay time, as observed in Figure 6A. In its normal growth and migration conditions, the wound closure was only ~40% after 16h (C^+). In this essay 2MH-P30 and P40 hydrogels composition seem to allow similar migration rate and wound closure, when compared to the control growth conditions C^+. At 24h, the cells' migration is also significantly lower than the observed migration in HEK, where only ~60% migration was observed under normal control growth conditions (C^+). However, 2MH-P30 maintains the same behaviour seen at 16h. Nonetheless, the P40 sample did not maintain its behaviour.

The assay revealed that migration of HEKs is very fast, having a coverage of ~87% of the wound after 16h, in normal conditions (C^+). Particularly, the P30 and 2MH-P30 patches composition, seem to provide a similar environment to its normal migration conditions. This means both the used components in the hydrogel base and the introduced honey concentration are not deleterious to the cells and its migration and proliferation abilities. P40 seem to have a delayed cell migration of about 40% at 16h. This could be due to the cells adaptation of the new materials present in the growth medium. After 24h, the wound scratch was fully closed in normal conditions (100%). The behaviour was maintained from 16h, where P30 and 2MH-P30 showed similar cell migration to the control and P40 showed a migration delay (~15%).

Comparing all the results, the assays showed significant variability between patches and between cell lines. However, the 2MH-P30 patch was the only one who maintained the same behaviour between cell lines and was able to provide a similar environment to the control, in every setting.

Although it was not possible to observe a higher cell migration with the incorporation of MH, as it has been previously described by other authors, it was possible to incorporate a much higher MH concentration than the described in the literature, without impairing cell viability.

Antioxidant Activity Assay

As previously mentioned, an excessive amount of reactive oxygen species (ROS) can be deleterious to the cells. Therefore, studying the antioxidant activity of the patches is of extreme importance (Figure 7).

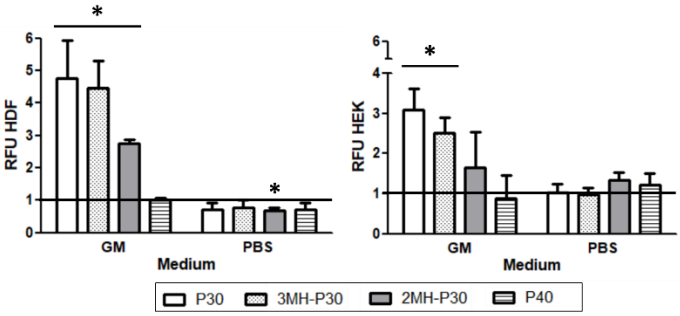

Figure 7 - Antioxidant activity of the 3D patches in human dermal fibroblasts (A) and human epidermal fibroblasts (B). The assay was performed under 2 conditions: cell incubation with the samples dissolved in growth medium (GM) and PBS (PBS). Results appear as relative fluorescence units (RFU) and the solid line is ascorbic acid (AA), the positive control, and corresponds to RFU=1. * - Significantly different from the positive control (AA), at the same time-point.

Since the growth media have ascorbic acid (AA) present in their composition, and since it is the used positive

control in this essay, the same conditions were also tested with the extracts being made in PBS.
When the extracts were prepared in PBS, the results are very uniform, for HDF and HEK, with no significant variance, when compared to ascorbic acid (AA).
In HDF the 2MH-P30 patch even seems to provide a slightly higher protection against ROS than AA. However, in the assay where the extracts were prepared in culture medium, more differences between samples and the control can be seen. First, for HDF, the sample that has more gelatine, P40, seem to have a higher antioxidant activity and similar to AA. It also provides a higher protection against ROS when in comparison with the P30, 3MH-P30 and 2MH-P30. The reduction in honey amount, from 3MH-P30 to 2MH-P30, increases the protection provided by the hydrogel against ROS, thus the latter has a higher antioxidant activity.
For HEK, 2MH-P30 and P40 patches have similar behaviour as the positive control, when incubated in growth medium. The increase in antioxidant activity observed by increasing honey concentration in HDF is no longer observed for HEK, since the results for 3MH-P30 and 2MH-P30 are not statistically different.
The results seem to suggest that the culture medium has an impact in the results, which is plausible since the media themselves have ascorbic acid present (the RFU value was like ascorbic acid), which could be interfering with the results. However, more differences were expected to be observed in the PBS essay, since the interference of AA was not present. Additionally, it would be expected that a higher honey concentration would provide a higher antioxidant activity to the hydrogel. But the opposite was observed for HDF. This can be explained by the previous cytotoxicity observed in HDF when incubated with 3MH-P30 extracts, also inducing a higher production of ROS by the cells.

Irritability and Angiogenesis Tests

For the final portion of this work, *in vivo* essays were performed, to test the irritability and angiogenic potential of the patches, respectively.
On the irritation potential assay (results not shown), the patches did not induce noticeable adverse vascular alterations, and the results were similar to the negative control (treatment with NaCl, 0.9%) and substantially different of the positive control (treatment with NaOH, 0.5M). None of the patches' composition significantly affected the angiogenic response (Figure 8) and behaved similarly after CAM maturation for 3 days, meaning they did not have a significant higher influence on the formation of new blood vessels.

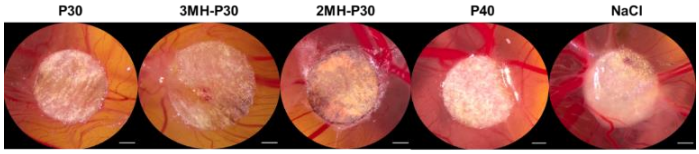

Figure 8 - *In vivo* HET-CAM angiogenesis essay. Angiogenic response to the embedded filter with the patches, evaluated by the CAM assay after 3 days post window creation. Microscopic images of the CAM exposed to the extracts and the negative control (0.9% NaCl) at 10x magnification, where scale bar is 2.5 mm .

4. Conclusion and Future Perspectives

Conclusion

In this work, the development of 3D printed gelatine-based hydrogels, incorporated with the bioactive agent Manuka honey (MH) was presented for applications in wound healing and skin regeneration. The main objectives of the work have been reached: (1) the production of reproducible 3D patches with printing accuracy and high shape fidelity; (2) the successful incorporation of MH in the developed 3D patches, whilst preserving its inherent properties, especially its antibacterial activity.
Additionally, mostly properties such as printing temperature, viscosity and excipients concentration showed to significantly influence the printing process and quality of the 3D patches. The temperature at which printing occurs, increased from 34 ºC for P30 ink to 43 ºC for MH-P30 and P40 inks. This increase in temperature occurs to avoid nozzle clogging and premature gelation of the ink inside the cartridge. In conclusion, the printing properties of the developed inks were found to be suitable for extrusion-based printing. Moreover, as observed in this study from drop tests, higher concentration of gelatine and the incorporation of MH allowed less filament spreading, a better printing accuracy, and consequently, more reproducible, and accurate patches.
Even though microscopically, MH-P30 and P40 patches appear to have similar morphology, SEM characterization showed that MH-P30 patches had more homogeneous filaments, between layers, contrary to P40. Both MH-P30 and P40 patches presented adequate size porous and high porosity, both desirable features in hydrogels for wound healing applications.
Antimicrobial activity of the printed patches was assessed, and as expected, the patches with honey incorporated caused an antibacterial effect on the gram-positive bacteria, *S. aureus* and *S. epidermidis*, and on the gram-negative bacteria *E. coli*. No effect was observed on *P. aeruginosa,* that could be caused by using a MH concentration (40%) very close to the obtained MIC and MBC for this bacterium (35.5 %). No significant differences were observed between the inhibition of 3MH-P30 and 2MH-P30. Agar diffusion assay confirmed the antimicrobial effect of MH.
Cell viability was also assessed in human dermal fibroblasts (HDF) and human epidermal keratinocytes (HEK) and the 3MH-P30 hydrogel showed to cause an inhibition of >50% in both cell lines. However, 2MH-P30 did not cause significant cytotoxicity in the cells. Moreover, it appeared to promote a higher proliferation and growth of HDF, compared to the control. It is possible to conclude, then, that the cells are sensitive to MH concentration, and that cellular tests should always be investigated, in parallel with the antimicrobial tests. Regarding the possible regeneration capacity by MH, although it was not possible to observe a higher cell migration with the incorporation of MH, a much higher MH concentration than the described in the literature was able to be incorporated, without impairing cell viability and proliferation. Moreover, the 2MH-P30 patch allowed a similar migration to normal conditions. A strong possible antioxidant activity may also be attained from the produced patches.
Finally, the *in vivo* HET-CAM irritability and angiogenesis tests, showed that the developed patches did not cause irritation and were also unable to promote angiogenesis.
Thus, the main goals of this project were achieved and was possible to produce 3D printed hydrogels that demonstrate great printability and reproducible results.

The added antibacterial substance, MH, showed successful results that justifies its application to improve hydrogel's effectiveness and regeneration ability.

Future Perspectives

One of the most important properties that a hydrogel should have is a good swelling capacity. To achieve a better understanding about its water absorption capability, a detailed study on the swelling ratio and water content of the developed 3D patches should be performed. It is also important that the produced patches are stable and do not degrade in a very fast paste. In the future, to define the degradation rate of the hydrogels seems important.

As it was previously stated, MH has a very high methylglyoxal (MGO) concentration, which as a huge impact in its antibacterial effect. However, it is known that other MH components also impact its antibacterial effect. Thus, it would be interesting to perform a detailed study on the chemical composition of the used MH and the effect of each component in the antibacterial activity. The incorporation of other antibacterial compounds to the gelatine-based hydrogel, in addition to MH, should also be considered, to create a synergistic antibacterial effect and to enhance the patch's therapeutic properties. As an example, the addition of metal nanoparticles, such as silver, zinc, and gold, are increasingly being used in wound healing applications. Moreover, another polymer such as chitosan could also be added. Besides its antibacterial activity, it also promotes wound healing and could potentially increase the mechanical properties of the hydrogel.

5. Acknowledgments

The author thanks 3DGelComp Group for providing the 3D printer; Bone Lab Research Group for the opportunity to develop the biological characterization work; Prof. Catarina Santos, Prof. Joana Marto, Prof. Maria Helena Fernandes, and Prof. Liliana Grenho for their supervision during the experimental work.

6. References

[1] A. Smandri, A. Nordin, N. M. Hwei, K. Y. Chin, I. Abd Aziz, and M. B. Fauzi, "Natural 3D-printed bioinks for skin regeneration and wound healing: A systematic review," *Polymers (Basel).*, vol. 12, no. 8, Aug. 2020.

[2] E. A. Kamoun, E. R. S. Kenawy, and X. Chen, "A review on polymeric hydrogel membranes for wound dressing applications: PVA-based hydrogel dressings," *J. Adv. Res.*, vol. 8, no. 3, pp. 217–233, May 2017.

[3] H. Liu *et al.*, "A functional chitosan-based hydrogel as a wound dressing and drug delivery system in the treatment of wound healing," *RSC Adv.*, vol. 8, no. 14, pp. 7533–7549, Feb. 2018.

[4] S. Tavakoli and A. S. Klar, "Advanced hydrogels as wound dressings," *Biomolecules*, vol. 10, no. 8. MDPI AG, pp. 1–20, Aug. 01, 2020.

[5] M. Di Giuseppe et al., "Mechanical behaviour of alginate-gelatin hydrogels for 3D bioprinting," J. Mech. Behav. Biomed. Mater., vol. 79, pp. 150–157, Mar. 2018, doi: 10.1016/J.JMBBM.2017.12.018.

[6] I. Iacopetti, A. Perazzi, T. Martinello, F. Gemignani, and M. Patruno, "Hyaluronic acid, Manuka honey and Acemannan gel: Wound-specific applications for skin lesions," *Res. Vet. Sci.*, vol. 129, pp. 82–89, Apr. 2020.

[7] V. C. Nolan, J. Harrison, J. E. E. Wright, J. A. G. Cox, "Clinical Significance of Manuka and Medical-Grade Honey for Antibiotic-Resistant Infections: A Systematic Review," *Antibiot. (Basel, Switzerland)*, vol. 9, no. 11, pp. 1–24, Nov. 2020.

[8] K. Schuhladen, P. Mukoo, L. Liverani, Z. Neščáková, A. R. Boccaccini, "Manuka honey and bioactive glass impart methylcellulose foams with antibacterial effects for wound-healing applications" IOP Publishing Ltd, Biomedical Materials, vol. 15, no. 6, September 2020.

[9] I. Wiegand, K. Hilpert, R. E. W. Hancock, "Agar and broth dilution methods to determine the minimal inhibitory concentration (MIC) of antimicrobial substances," *Nat. Protoc.*, vol. 3, no. 2, pp. 163–175, Feb. 2008.

[10] S. B. Almasaudi et al., "Antimicrobial effect of different types of honey on Staphylococcus aureus," Saudi J. Biol. Sci., vol. 24, no. 6, pp. 1255–1261, Sep. 2017.

[11] S. hui Hsu and A. M. Jamieson, "Viscoelastic behaviour at the thermal sol-gel transition of gelatin," *Polymer (Guildf).*, vol. 34, no. 12, pp. 2602–2608, Jan. 1993.

[12] V. Kokol, Y. B. Pottathara, M. Mihelčič, and L. S. Perše, "Rheological properties of gelatine hydrogels affected by flow- and horizontally-induced cooling rates during 3D cryo-printing," *Colloids Surfaces A Physicochem. Eng. Asp.*, vol. 616, p. 126356, May 2021.

[13] F.-F. Cai, S. Heid, and A. R. Boccaccini, "Potential of Laponite® incorporated oxidized alginate–gelatin (ADA-GEL) composite hydrogels for extrusion-based 3D printing," *J. Biomed. Mater. Res. Part B Appl. Biomater.*, vol. 109, no. 8, pp. 1090–1104, Aug. 2021.

[14] S. W *et al.*, "Gelatin-methacrylamide hydrogels as potential biomaterials for fabrication of tissue-engineered cartilage constructs," *Macromol. Biosci.*, vol. 13, no. 5, pp. 551–561, May 2013.

[15] T. Jiang, J. G. Munguia-Lopez, S. Flores-Torres, J. Kort-Mascort, and J. M. Kinsella, "Extrusion bioprinting of soft materials: An emerging technique for biological model fabrication," *Appl. Phys. Rev.*, vol. 6, no. 1, p. 011310, Mar. 2019.

[16] S. Bom et al., "Effects of starch incorporation on the physicochemical properties and release kinetics of alginate-based 3D hydrogel patches for topical delivery," Pharmaceutics, vol. 12, no. 8, pp. 1–20, Jul. 2020, doi: 10.3390/pharmaceutics12080719.

[17] D. J. Choi, S. J. Park, B. K. Gu, Y. J. Kim, S. Chung, and C. H. Kim, "Effect of the pore size in a 3D bioprinted gelatin scaffold on fibroblast proliferation," *J. Ind. Eng. Chem.*, vol. 67, pp. 388–395, Nov. 2018.

[18] A. Girma, W. Seo, and R. C. She, "Antibacterial activity of varying UMF-graded Manuka honeys," *PLoS One*, vol. 14, no. 10, Oct. 2019.

[19] "ISO - ISO 10993-5:2009 - Biological evaluation of medical devices — Part 5: Tests for in vitro cytotoxicity." https://www.iso.org/standard/36406.html (accessed Oct. 27, 2021).

[20] K. R. Hixon, T. Lu, S. H. McBride-Gagyi, B. E. Janowiak, and S. A. Sell, "A comparison of tissue engineering scaffolds incorporated with Manuka honey of varying UMF," *Biomed Res. Int.*, vol. 2017, 2017.

[21] S. Patel, S. Srivastava, M. R. Singh, and D. Singh, "Preparation and optimization of chitosan-gelatin films for sustained delivery of lupeol for wound healing," *Int. J. Biol. Macromol.*, vol. 107, pp. 1888–1897, Feb. 2018.

[22] T. Goodpaster, A. Legesse-Miller, M. R. Hameed, S. C. Aisner, J. Randolph-Habecker, and H. A. Coller, "An Immunohistochemical Method for Identifying Fibroblasts in Formalin-fixed, Paraffin-embedded Tissue," *J. Histochem. Cytochem.*, vol. 56, no. 4, p. 347, Apr. 2008.

[23] I. Miller *et al.*, "Ki67 is a Graded Rather than a Binary Marker of Proliferation versus Quiescence," *Cell Rep.*, vol. 24, no. 5, p. 1105, Jul. 2018.

[24] E. Hunter-Featherstone *et al.*, "Culturing Keratinocytes on Biomimetic Substrates Facilitates Improved Epidermal Assembly In Vitro," *Cells 2021, Vol. 10, Page 1177*, vol. 10, no. 5, p. 1177, May 2021.